Meta-microwindmill structure used as absorber layer to detect ketamine and amphetamine type stimulants in terahertz domain

Shun Cao[1, 2], Weixing Yu[1, *], Taisheng Wang[1], Honghai Shen[1], Xudong Han[1], Wenbin Xu[1], Xuming Zhang[3]

[1]State Key Laboratory of Applied Optics, Changchun Institute of Optics, Fine Mechanics & Physics, Chinese Academy of Sciences, No.3888, Dongnanhu Road, Changchun,

Jilin, P.R. China

[2]University of the Chinese Academy of Sciences, Beijing, 10039, P.R. China

[3]Department of Applied Physics, Hong Kong Polytechnic University, Hung Hom,

Kowloon, Hong Kong

*[*yuwx@ciomp.ac.cn*](mailto:yuwx@ciomp.ac.cn)

Abstract: We report a metamaterial based microwindmill array with a periodic arrangement that can be used in terahertz detector as an absorbing layer. It is found that this structure can absorb terahertz waves efficiently with an average absorptivity of 95% at multiple wavelengths of 1.516THz, 2.205THz, 2.424THz, and 2.565THz, which are absorption peaks of spectra for four kinds of drugs respectively. The efficient absorbing property of meta-microwindmill on terahertz wave can be explained in terms of the synergetic effects of localized surface plasmon resonant effect and slow light mode. Moreover, the effect of the error of the structural parameters on the absorption efficiency has been carefully analyzed to guide the process of the fabrication.

OCIS codes: (040.0040) Detectors; (110.6795) Terahertz imaging; (160.3918) Metamaterials; (260.5740) Resonance;

References and links

1. F. Oliveira, R. Barat, B. Schulkin, F. Huang, J. Federici and D. Gary, "Neural network analysis of terahertz spectra of explosives and bio-agents," Proc. SPIE 5070, 60–70 (2003).
2. J. F. Federici, B. Schulkin, F. Huang, D. Gary, R. Barat, F. Oliveira and D. Zimdars, "THz imaging and sensing for security applications - explosives, weapons, and drugs," Semicond. Sci. Technol. **20**, S266–S280 (2005).
3. H.-B. Liu, Y. Chen, G. J. Bastiaans and X.-C. Zhang, "Detection and identification of explosive RDX by THz diffuse reflection spectroscopy," Opt. Express **11**, 2549–2554 (2003).
4. A. W. M. Lee, Q. Hu, "Real-time, continuous-wave terahertz imaging by use of a microbolometer focal-plane array," Opt. letters **30**(19), 2563–2565 (2005).
5. A. W. M. Lee, B. S. Williams, S. Kumar, Q. Hu, J. L. Reno, "Real-time imaging using a 4.3-THz quantum cascade laser and a 320×240 micro-bolometer focal plane array," IEEE Photon. Technol. Lett. **18**(13), 1415–1417 (2006).
6. N. Oda, H. Yoneyama, T. Sasaki, M. Sano, S. Kurashina, I. Hosako, N. Sekine, T. Sudoh and T. Irie, "Detection of terahertz radiation from quantum cascade laser, using vanadium oxide microbolometer focal plane arrays," Proc. SPIE 6940, 1–12 (2008).
7. N. Oda, M. Sano, K. Sonoda, H. Yoneyama, S. Kurashina, M. Miyoshi, T. Sasaki, I. Hosako, N. Sekine, T. Sudou and S. Ohuichi, "Development of terahertz focal plane arrays and handy camera," Proc. SPIE 8012, 1–9 (2011).
8. N. Oda, A. W. M. Lee, T. Ishi, "Proposal for real-time terahertz imaging system with palm-size terahertz camera and compact quantum cascade laser," Proc. SPIE 8363, 1–13 (2012).

9. F. Simoens, A. Arnaud, P. Castelein, V. Goudon, P. Imperinetti, J. Lalanne Dera, J. Meilham, J. L. Ouvier Buffet, S. Pocas, T. Maillou, L. Hairsult, P. Gellie, S. Barbieri, C. Sirtori, "Development of uncooled antenna-coupled microbolometer array for explosive detection and identification," Proc. SPIE 7837,1–11 (2010).
10. J. Pendry, "Negative refraction makes a perfect lens," Phys. Rev. Lett. **85**(18), 3966–3969 (2000).
11. D. Schurig, J. Mock, B. Justice, S. Cummer, J. Pendry, A. Starr, and D. Smith, "Metamaterial electromagnetic cloak at microwave frequencies," Science **314**(5801), 977–980 (2006).
12. N. Fang, H. Lee, C. Sun, and X. Zhang, "Sub–diffraction-limited optical imaging with a silver superlens," Science **308**(5721), 534–537 (2005).
13. J. Valentine, S. Zhang, T. Zentgraf, E. Ulin-Avila, D. Genov, G. Bartal, and X. Zhang, "Three-dimensional optical metamaterial with a negative refractive index," Nature **455**(7211), 376–379 (2008).
14. X. Shen, T. J. Cui, J. Zhao, H. F. Ma, W. X. Jiang, and H. Li, "Polarization- independent wide-angle triple-band metamaterial absorber," Opt. Express **19**, 9404–9407 (2011).
15. P. Ding, E. Liang, G. Cai, W. Hu, C. Fan and Q. Xue, "Dual-band perfect absorption and field enhancement by interaction between localized and propagating surface plasmons in optical metamaterials," J. Opt. **13**, 075005 (2011).
16. S. Cao, W. Yu, T. Wang, Z. Xu, C. Wang, Y. Fu and Y. Liu, "Two-dimensional subwavelength meta-nanopillar array for efficient visible light absorption," Appl. Phys. Lett. **102**(16): 161109 (2013).
17. Z. H. Jiang, S. Yun, F. Toor, D. H. Werner, and T. S. Mayer, "Conformal dual-band near-perfectly absorbing mid-infrared metamaterial coating," Nano **5**, 4641–4647 (2011).
18. Q. Liang, T. Wang, Z. Lu, Q. Sun, Y. Fu, and W. Yu, "Metamaterial-based two dimensional plasmonic subwavelength structures offer the broadest waveband light harvesting," Adv. Opt. Mater. **1**(1), 43–49 (2013).
19. Y. Ma, Q. Chen, J. Grant, S. C. Saha, A. Khalid, and D. R. S. Cumming, "A terahertz polarization insensitive dual band metamaterial absorber," Opt. Lett. **36**, 945–947 (2011).
20. Tao, N. Landy, C. Bingham, X. Zhang, R. Averitt, and W. Padilla, "A metamaterial absorber for the terahertz regime: Design, fabrication and characterization," Opt. Express **16**, 7181–7188 (2008).
21. N. I. Landy, S. Sajuyigbe, J. J. Mock, D. R. Smith and W. J. Padilla, "Perfect metamaterial absorber." Physical review letters **100**, 207402 (2008).
22. D. Cheng, J. Xie, H. Zhang, C. Wang, N. Zhang, and L. Deng, "Pantoscopic and polarization-insensitive perfect absorbers in the middle infrared spectrum," JOSA B **29**(6), 1503–1510 (2012).
23. J. Hao, J. Wang, X. Liu, W. J. Padilla, L. Zhou, and M. Qiu, "High performance optical absorber based on a plasmonic metamaterial," Applied Physics Letters, **96**(25), 251104 (2010).
24. Y. Cui, J. Xu, K. Fung, Y. Jin, A. Kumar, S. He, X. Fang, "Ultrabroadband light absorption by a sawtooth anisotropic metamaterial slab," Nano Lett. **12**, 1443–1447 (2012).

1. Introduction

The progress of terahertz detectors, which is the essential device of the terahertz imaging system, plays an important role in the development of terahertz imaging technology. With many unique properties, the terahertz wave detector could be used in security imaging [1,2,3]. After many years' efforts, infrared focal plane array (FPA) detector technology has been well developed. Although it was reported that FPA detector can be used for terahertz wave detection directly recently, many efforts have been devoted to improve its sensitivity and resolution [4-9]. Alan W.M. Lee *et al* designed CW THz transmission imaging systems working on 2.52THz and 4.3THz by using microbolometer camera and demonstrated that microbolometer could be used directly for terahertz imaging, despite the poor sensitivity of the microbolometer at the terahertz wave band [4,5]. Naoki Oda *et al* added the thin metallic film, acting as terahertz absorption layer, to match the optical resonance cavity above the vanadium oxide microbolometer focal plane arrays and realized the real-time imaging of THz radiation [6,7,8]. However, this thin metallic film could not absorb terahertz wave efficiently at the terahertz spectra.

Metamaterials are one potential solution to solve this problem. Metamaterials are unnatural materials composed of metallic/dielectric micro/nanostructures and they have recently attracted increasing attentions, for their exotic electromagnetic responses [10-13]. Various metamaterial-based absorbers have been developed to work efficiently at wavebands ranging from microwave [14], visible [15,16], infrared [17,18] to terahertz [19]. In this work, we designed a metamaterial-based absorber with multiple absorption peak in terahertz

waveband for the purpose of detecting the featured absorption peak of various drugs: ketamine and three typical amphetamine type stimulants (MATM, MDMA and MDA), whose absorption peaks locate at 1.52THz, 2.21THz, 2.43THz and 2.57THz, respectively, the working frequency band for the designed absorber is chosen as 1.4 – 2.7 THz. To detect these four drugs simultaneously, a meta-microwindmill terahertz absorber that has four high efficient absorption peaks at above four featured frequencies is designed. The absorption mechanism of the absorber is numerically investigated and the influence of the error of absorber structural parameters on the absorbing efficiency is also analyzed.

2. Metamaterial-based microwindmill efficient terahertz absorber

To achieve a high absorbing efficiency at multiple THz frequencies, a metamaterial based microwindmill terahertz absorber was designed. The schematic diagrams are shown in Fig. 1. Fig.1(a) shows the top view of the layout of one unit cell of the meta-microwindmill absorber. Basically, there are four sets of rectangular and fan structures with different sizes. Fig.1(b) shows the cross sectional view of the absorber. As can be seen, it consists of three layers: metal/dielectric/metal. The microwindmill structure is fabricated in the top metallic film, which is actually an electrical ring resonator (ERR), i.e. a common part of the metamaterials structures [20,21]. The dielectric layer sandwiched in between two metallic layers actually provides a resonant space for the Fabry-Pérot (F-P) resonator. The metallic film on the bottom normally should be thick enough so that it is opaque to the working waveband. In this way, the proposed metamaterial based absorber consists of an electrical ring resonator and an F-P resonator. By employing this hybrid resonator structure, one can achieve a highly efficient absorption at a broad waveband with multiple absorption peaks. For the terahertz wave focal plane detector, the absorbed electromagnetic energy is converted into heat first and then the heat is converted into electronic current by the infrared FPA detector.
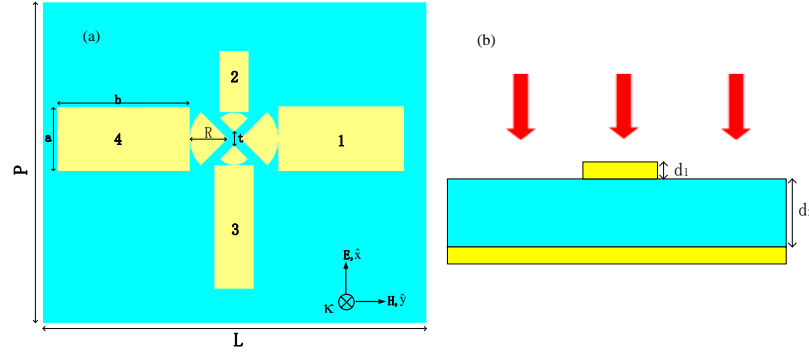

Fig. 1. Schematics of meta-microwindmill terahertz absorber: (a) microwindmill structure on the top of a polyimide spacer and one unit cell showing the direction of propagation of incident EM waves; (b) cross-sectional view of the unit cell. The wide (L) and length (P) of unit cell is L=144μm and P=120μm, respectively.

By employing the commercial finite-difference time domain (FDTD) software package (Lumerical FDTD Solutions), the meta-microwindmill structure was modeled and analyzed. The three-dimensional simulations were performed with a plane wave source incident in the z direction (see the inset of Fig.1(a)). Periodic boundary conditions were employed for both x and y directions and PML boundary condition was employed in z direction. The inset of Fig.1(a) shows the direction of incident terahertz EM waves with respect of the cross section of the designed absorber. Aluminum is selected as metal layer and its conductivity is σ=3.56×10^{7}S/m and polyimide is selected as dielectric layer with $\tilde{\varepsilon} = 3.5 + i0.02$. The absorptivity was calculated by using the equation $A(\lambda)$=1-$R(\lambda)$-$T(\lambda)$, where $R(\lambda)$=|S_{11}|^2 is the reflection and $T(\lambda)$=|S_{21}|^2 is the transmission. Since the thickness of the bottom metal plane

(d_1= 200 nm) is much larger than its typical skin depth, there is nearly no transmittance in the overall frequency range, i.e. $T(\lambda)$=0. In this case, the formulation used to calculate the absorptivity is simplified into $A(\lambda)=1-R(\lambda)$.

For impedance matching, the thicknesses of the metal and dielectric layer should be optimized so that the maximum absorption can be achieved. In simulations, the thickness of the top metal d_1=200nm, which has the same thickness with that of the ground metal plane [22]. On the other hand, the thickness of the dielectric film also affects the absorption performance, because it influences the terahertz wave interaction in between the adjacent metal layers. In the metamaterial-based microwindmill terahertz absorber, the optimal thickness of polyimide layer (d_2) is found to be d_2=8 μm. Next, the structural parameters of the microwindmill is optimized so that the targeted frequencies of the terahertz wave resonate with it to achieve the highest absorption in these frequencies. The radius (R) of the central microfan for subunit 1 – 4 is 11.12 μm, 9.7 μm, 9.7 μm and 11.12 μm, respectively. The gap between the opposite microfans is t=5 μm. These parameters are chosen in microscale so that the microstructure can be realized by the normal photolithography. The optimized width (a) and length (b) of the rectangles for four subuints are listed in Table 1.

Table 1. Optimized width (a) and length (b) of the rectangles for four subuints of the microwindmill structure.

Part	a/μm	b/μm
1	22.4	45.0
2	8.0	23.5
3	14.0	45.0
4	24.7	47.7

Frequency domain solver was used to investigate the S-parameters of transmission (S_{21}) and reflection (S_{11}) of a single unite cell. Fig.2(a) shows the reflection (R), transmission (T) and absorption (A) against the frequency for normal incident terahertz wave. As can be seen clearly, the absorption curve has four peaks at 1.516THz (98.1%), 2.205THz (91.8%), 2.424THz (95.6%) and 2.565THz (99.9%), respectively. Apparently, the average absorptivity at the targeted four frequencies is 96.35%. At particularly 2.565THz, close to the 2.57THz resonant frequency, we have achieved nearly unity absorption. Fig. 2(b) shows the performance at different incident angles of the terahertz wave. One can see that the incident angle has great impact on the absorptivity as well as the absorption peak position. When the incident angle increases, the absorptivity at peaks of 1.52THz and 2.43THz reaches nearly unity. However, the absorption at peaks of 2.21THz and 2.57THz drops significantly to less than 70% (2.21THz) and 80% (2.57THz), respectively. Moreover, with the increase of the incident angle, the position of the absorption peaks also changes and has a blue shift. In general, the shift degree is proportional to the reduction of absorption. As can be seen clearly, the shift at frequency is largest (about 0.069 THz) and the reduction of absorption at this frequency is also the largest (about 27.3%). Consequently, this meta-microwindmill structure becomes inefficient to absorb terahertz wave when the incident angels are more than 30°, due to the asymmetry of the designed structure.
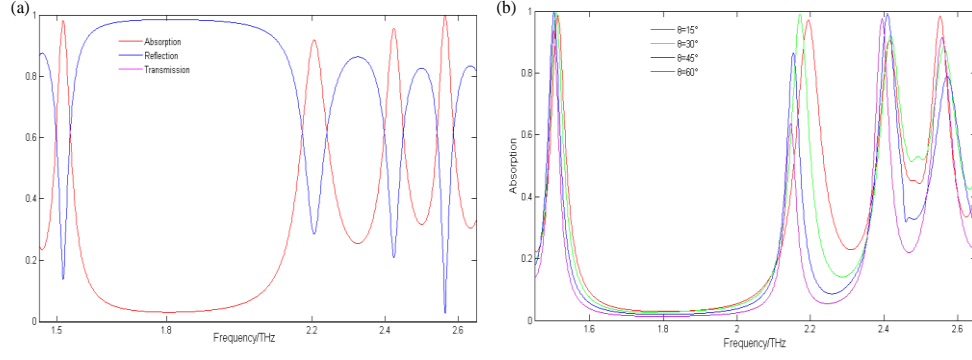
Fig. 2. Absorption spectra of the meta-microwindmill absorber. (a) Absorption (red), reflection (blue) and transmission (pink) against frequency for normal incident terahertz wave; (b) Absorption against frequency for different incident angles of 15°, 30°, 45°, 60° for TM wave.

3. Numerical investigation of the absorption mechanism

The physical mechanism of the meta-microwindmill terahertz absorber was analyzed. We first investigated the power density distribution (see Fig. 3) and the electric energy density distribution (see Fig. 4) in the plane of z=0μm (the interface between the top metal layer and the dielectric layer) at four resonant frequencies for the TM polarized wave. As shown in Fig.3, the energy density is concentrated mainly at the edges of the fans and the rectangles. For 1.516THz, subunit 3 absorbs much more energy than the other subunits. Therefore, subunit 3 mainly contributes to the absorption of this frequency. Similarly, subunit 2, 4 and 1 mainly contributes the absorptions of 2.205THz, 2.424THz and 2.565THz, respectively. Of course, for some frequencies, other subunits also contribute to the absorption to some extent besides the main contributing subunit. For instance, at frequency 2.424THz, subunit 3 also contributes a portion of energy absorption besides the main contributing subunit 4. We can see that part 2 and part 3 get high absorption more independently than another two parts. And power loss density enhance on more area, higher absorption can be achieved.
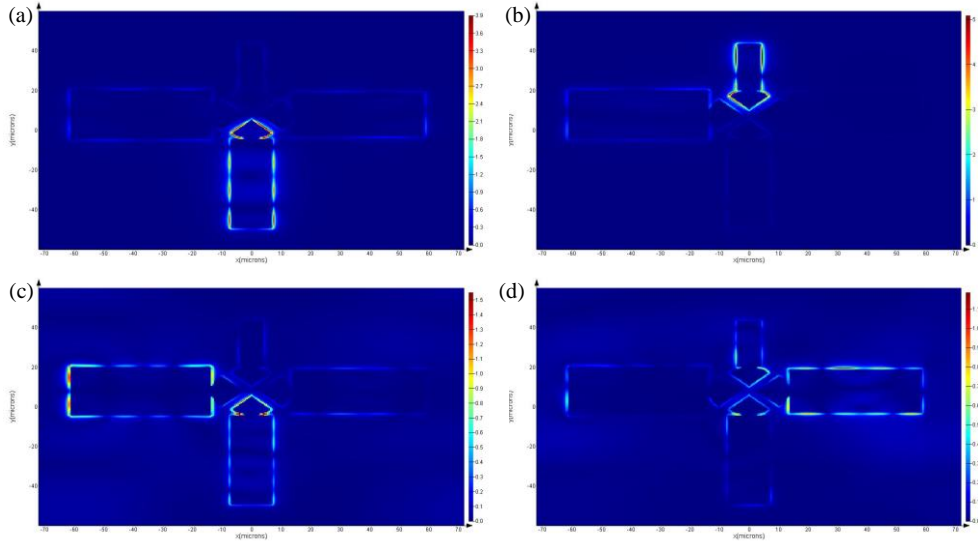

Fig. 3. Distribution of power density for the metamaterial microwindmill absorber in the plane z=0 μm at four resonant frequencies. (a) 1.516THz, (b) 2.205THz, (c)2.424THz and (d) 2.565THz, respectively.

5
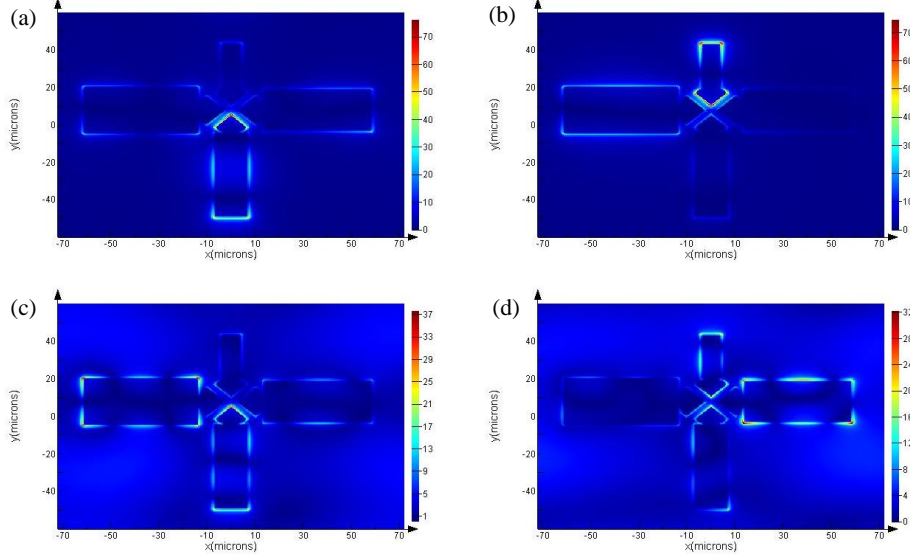
Fig. 4. Distribution of electric density for the metamaterial microwindmill absorber in the plane z=0μm at four resonant frequencies. (a) 1.516THz, (b) 2.205THz, (c)2.424THz and(d) 2.565THz, respectively.

From Fig.4, we can clearly observe that the electric energy hot spots are located mainly at corners of the microfans and the microrectangles. The sharper the corner is, the stronger the hot spot is. The hot spots mean the areas in which the electric field is greatly enhanced. We attribute this phenomenon to the localized surface plasmon resonance effect. And these hot spots' locations are close to those of power loss density distribution in Fig.3. As a result, the local excitation of surface plasmon resonance leads to the energy loss in the interface of metal/dielectric [23]. In order to prove these hot spots are induced by surface plasmon wave, the electric energy density and power loss density along z direction at 1.516THz resonant frequency under subunit 3 is calculated and plotted in Fig.5. As shown in Fig.5(a), the electric energy density at z=0 μm (the interface of metal/dielectric) is about two folds of that at z=0.2 μm (the interface of metal/air). Both electric energy density drops exponentially when the wave propagates away from metal surface into air or into dielectric of polyimide, which is the signature mark of surface plasmon wave. Fig.5(b) shows that the power loss density is greatly enhanced in the plane z=0 μm. Once the terahertz wave propagates into the dielectric layer, the energy drops exponentially to zero before it reaches the bottom layer of metal as shown in Fig.5(b1). In other words, the majority of the energy is absorbed in the metal layer and the rest is confined and stored inside the dielectric layer. The absorption of the energy inside the dielectric layer sandwiched between two metal layers can be attributed to the F-P resonant effect. Therefore, it is concluded that both the surface plasmon resonance and the F-P resonance contribute to the high absorption of the terahertz wave for the microwindmil absorber. The former plays the main role and together with the latter to achieve an ultrahigh resonant absorption. The energy loss density at the same point at nonresonant frequency 2THz was also analyzed and is shown in Fig.5(c). As can be seen, although the energy at z=0 μm is enhanced as well, but the intensity is three orders of magnitude lower than that at resonant frequency 1.516THz. Though the energy density is enhanced again at z = -0.43 μm, it is still much smaller than that at 1.516THz. From Fig.2(a), the absorption at 2THz is less than 10%. Hence, one can conclude that the localized surface plasmon resonance is the main reason for the high absorption at the resonant frequencies.
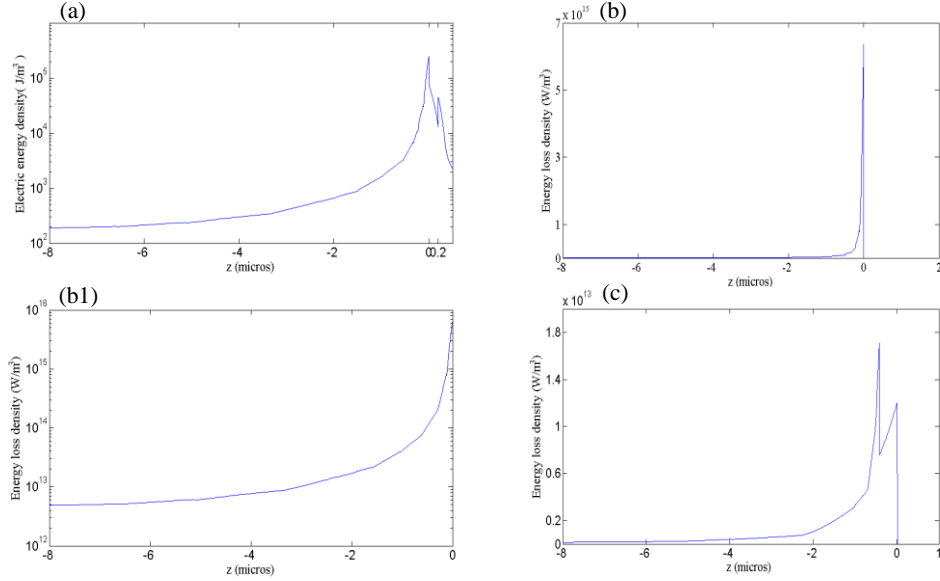
Fig. 5. Electric energy density and energy loss density of the meta-microwindmill absorber along z axis under the subunit 3. (a) electric energy density, (b) energy loss density, (b1) detail view of energy loss density in the dielectric layer at 1.516THz resonant frequency, (c) energy loss density at 2THz nonresonant frequency.
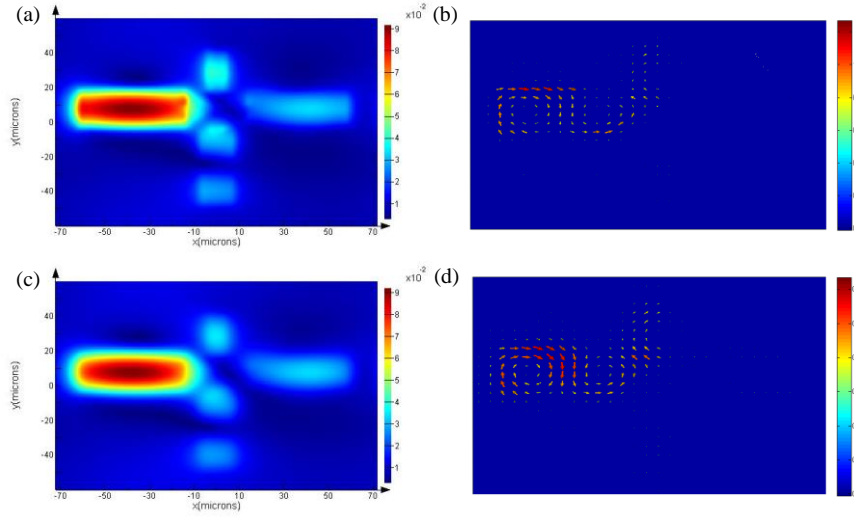

Fig. 6. Distributions of the normalized magnetic field and the energy flow for the microwindmill absorber in the plane of $z = -2$ μm and -4 μm at 2.424THz. (a) magnetic energy distribution in the plane of $z = -2$ μm, (b) energy flow distribution in $z = -2$ μm, (c) magnetic energy distribution in $z = -4$ μm, (d) energy flow distribution in $z = -4$ μm.

To further understand the absorbing mechanism in the dielectric layer of the metamaterial microwindmill structure, the energy flow distribution and the normalized magnetic field distribution in the plane of $z = -2$ μm and -4 μm at 2.424THz resonant frequency were investigated (see Fig.6). As shown in Fig.6(a) and (c), the magnetic field in the center of subunit 4 is the strongest. Furthermore, one can find that the magnetic energy density in the plane of $z = -2$ μm is similar to it in plane of $z = -4$ μm. As shown in Fig.6(b) and (d), energy

flow slowly converges and becomes energy vortex. In addition, the maxima magnetic distribution is in the center of the energy vortex, and this should be mainly attributed to slow light mode effect [24]. This effect enhances the interaction between terahertz wave and dielectric layer to help the absorber to absorb more energy at the resonant frequency.

Therefore, considering the results shown in Fig.5 and 6 and the discussions mentioned above, we can conclude that the physical mechanism for the strong absorption of metamaterial microwindmill absorber is the synergistic effect of localized surface plasmon enhancement, F-P resonant and slow light mode effect. Among them, surface plasmon resonant plays the main roles for the absorption of the energy in the interfaces of air/metal and metal/dielectric. The F-P resonance and the slow light effect contribute to the absorptions of remaining energy.

4. Effect of the fabrication errors on absorption

Fabrication errors can not be avoided so that the optimum design of microwindmill structure can not be perfectly fabricated in reality. In particular for the sharp corners in the microfan and microrectangles, the round shape corners are always formed in those locations. To evaluate the effect of the fabrication errors on absorption, we took errors for two parameters: the gap between one pair of the opposite subunits (t) and the radius at the vertex of the mcirofan.

Fig.7(a) shows the absorption against frequency for different gaps (t) of 7 μm, 9 μm, 11 μm and 13 μm between the opposite subunits. From Fig. 7(a), it can be found that the change of t has different effect on different resonant frequencies. For 1.52THz, both absorption and resonant frequency almost do not change for different gaps between subunits. For 2.57THz, the absorptivity slightly changes, i.e. no more than 5%. However, for 2.205THz and 2.43THz, when t changes from 7μm to 13μm, the absorption reduces significantly and the absorption peak frequency has an obvious blue shift. Therefore, in order to make sure the absorption at four targeted frequencies is all larger than 80%, the gap (t) between the opposite subunits should be no more than 9 μm.
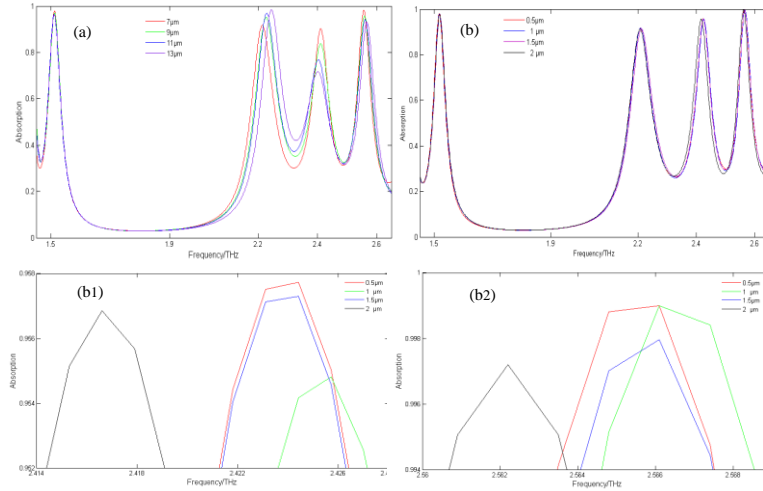

Fig.7. Absorption spectra of meta-microwindmill absorber under different parameters errors. (a) Under different gaps between the opposite subunits (t) (when r=0 μm); (b) Under different radius (r) at the vertex of the microfan (when t=5 μm); (b1) Detailed view of absorption peak at around 2.43THz in Fig.7(b); (b2) Detailed view of absorption peak at around 2.57THz in Fig.7(b).

Fig.7(b) shows the effect of the radius (r) at the vertex of the microfan on the absorption. The radius (r) is changed from 0.5 μm to 2 μm with a step size of Δr=0.5 μm. As can be seen, there is almost no change for the absorption when the radius changes. To look into the details,

the absorption curves at two peaks (2.43THz and 2.57THz) are magnified and shown in Fig.7(b1) and (b2). From Fig.7 (b1) and (b2), we can find that the summits of the absorption fluctuate less than 4% and the shifts of the resonant frequency are no more than 0.01THz. This is an advantage for the mask fabrication in that less processing accuracy is required to fabricated the structure of microfans.

5. Conclusions

In summary, we have designed an efficient terahertz multiband metamaterial absorber which can achieve over 91% absorption at all four targeted resonant frequencies. And these frequencies are close to the absorption spectra of the four drugs from 1.4THz to 2.7THz. The high absorptivity of the proposed absorber can be explained by the synergistic effect of the localized surface plasmon resonance enhancement, the Fabry-Perot resonant and the slow light effect. The error analyses of different structural parameters show that the error of the gap between subunits has a great effect on the absorbing performance but the radius of the vertex of the microfan has nearly no effect. Our next step will focus on the fabrication of the proposed absorber and then apply it for terahertz pyroelectric detector to detect four drugs.

5. Acknowledgement